Bidirectional Radiative Characteristics of Finite Clouds and Asian Dust (Kosa)

Kazuo Gotoh*, Tetsu Sakai, Takashi Shibata and Yasunobu Iwasaka

1. INTRODUCTION

Kosa (Yellow Sand), wind-blown mineral dust originating from the arid deserts of the Eastern Eurasian continent, is a meteorological phenomenon ushering in the springtime throughout East Asia, which is often cited in historical documents. In Japan, which is located thousands of kilometers away from its sources, Kosa did not mean anything more than a phenomenon representing the spring in old literatures, although in China and Korea, which are closer to the sources, it has had more meaning than that, and has often been regarded as life and health hazards.

Nowadays, however, the Kosa phenomenon has come to be considered to have other implications as the global environmental issues emerged. More often than not, the scale of the dust plume is such that it is transported across the Pacific reaching North America within several days. A heavy dust loading in the atmosphere can have negative or positive global warming effects. More over, anthropogenic chemicals brought about by growing industrial activities in this region have the potential to affect the global ecosystem. They are carried away by the same wind from the continent as Kosa to reach over Japan. Here, each particle of Kosa can directly react with such chemicals or can function as catalyst by providing chemical reaction fields on its surface. Also, it can function as a carrier in the process of deposition. Thus, there is a need to quantitatively understand the behavior of Kosa, especially of its spatial and temporal distributions, in other words, how it is transported to other regions.

*Corresponding author address: Solar-Terrestrial Environment Laboratory, Nagoya University
Furo-cho, Chikusa-ku, 464-0814 Nagoya, JAPAN
e-mail: kgotoh@nagoya-u.ac.jp

Geostationary satellites provide image data that are available at relatively short time intervals, allowing us to observe temporal developments of clouds and dust plumes, in which Kosa events are often seen associated with the clouds of low pressure systems. However, the sensors aboard such satellites have generally low resolutions, thus making identification of subpixel objects, such as cloud and Kosa, difficult.

Although good enough techniques for detection of dust distribution on satellite images have yet to be established, observations of ground-based lidar, another remote sensing method, have given us a good insight into the temporal change of dust structures in the atmosphere. There is possibility that as a method to discern dust aerosol from clouds, we can utilize the differences in their radiative characteristics, which result from the differences in the form of their presence in atmosphere. In the present study, radiative properties including reflection functions of both finite clouds and suspending dust seen in Kosa event is calculated by simulating photon scatters based on a radiative transfer model by the Monte Carlo method. In the simulation, no absorption in each scattering event is assumed. The spatial distributions of the Asian dust derived from lidar observations are exploited in the calculation. As for radiative properties of clouds, cumulus clouds are considered as a representative of finite clouds.

2. LIDAR OBSERVATION OF KOSA

The lidar system operated in Nagoya consists of a Nd:YAG laser oscillator, a Cassegrain telescope with 1000 mm diameter, and a multichannel photon-counter. Raman scattering lights of O_2, and H_2O are also detected simultaneously to estimate atmospheric temperature and relative humidity. The mixing ratio of atmospheric aerosol is obtained by taking ratio of Mie back scattering signal and Rayleigh back scattering signal.

The depolarized component in backscattering light from Rayleigh scattering of atmospheric molecules is extremely low. However, the same value from nonspherical particles is noticeably high, and therefore they can be easily detected by the depolarization ratio.

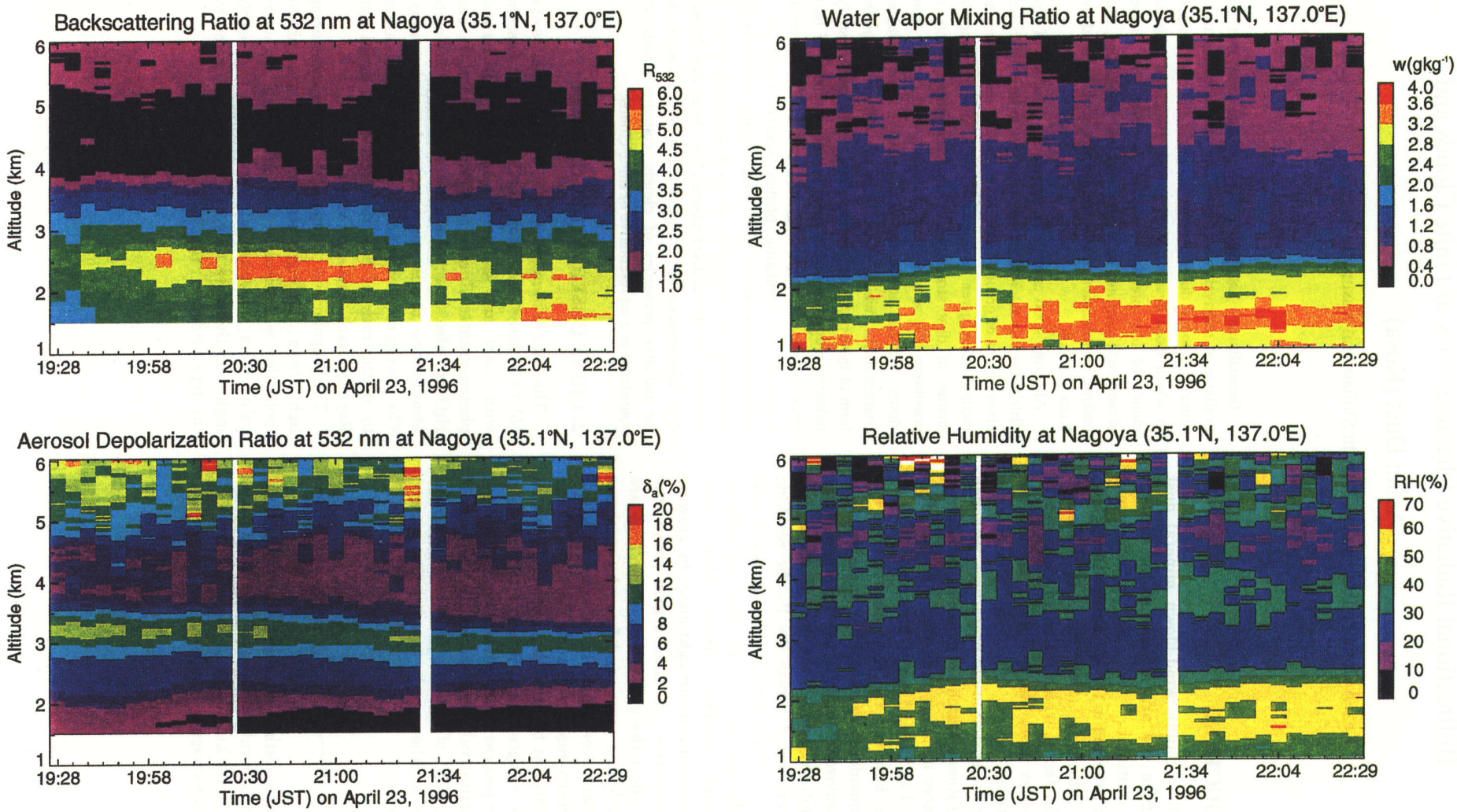

Fig. 1 Time-height cross section of backscattering ratio, depolarization ratio, watervapor mixing ratio, and relative humidity measured on April 23, 1996 in Nagoya

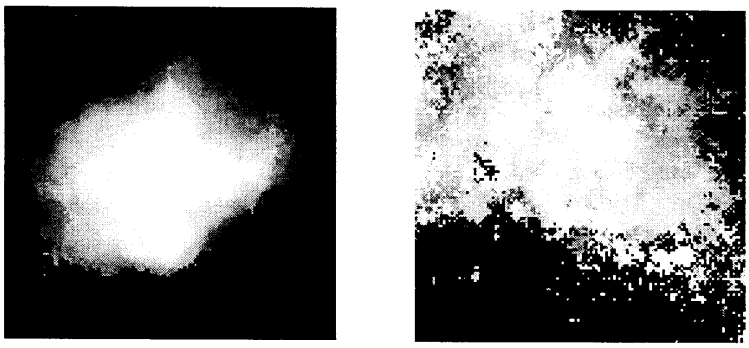

$H = 0.67$
$D_f = 1.33$

$H = 0.2$
$D_f = 1.8$

Fig. 2 The vertical view of the synthesized fractal clouds. Brightness denote the height of the cloud surface.

Angstrome exponent is also determined by measuring backscattering signal from aerosol at both 532 and 1064 nm.

Finally, volume extinction coefficient should be obtained for the Monte Carlo photon transport simulation. Since it is impossible to solve the Lidar equation for extinction coefficient only by the values mentioned above, iterative calculation is performed until all the values converge.

In Fig. 1, temporal developments of back scattering ratio, aerosol depolarization ratio, water vapor mixing ratio and relative humidity on the night of April 23, 1996 are shown. As seen in the figure, there is an apparent aerosol layer at around 2.5 to 3 km with high back scattering ratio. Based on the fact that depolarization ratio is high and relative humidity is low at this particular altitude, this layer is assumed to be a Kosa layer, not cloud layer. Extinction coefficient is calculated for this layer, and a Kosa layer model based on it was made for the photon transport simulation.

3. CUMULUS CLOUD MODEL

Real cloud fields appear quite complex in the spatial structure of the clouds. Clouds' structural complexity is often described using fractal dimension, which Lovejoy (1982) have found by adopting Mandelbrot's fractal theory (1974) to the cloud self affinity geometry using images taken by satellites. In this study, the cumulus cloud model used in the photon tracing simulation is assumed to have fractal geometry.

A variant of the midpoint displacement procedure is applied to generate a cloud with fractal scaling nature. The midpoint displacement procedure can be explained simply by taking the example of 1-dimensional brownian motion (Feder, 1988). Assuming that two separate points, $x(t)$ and $x(t+\delta_0)$, are initially placed. The midpoint $x(t+1/2\delta_0) = x(t+\delta_1)$ is generated from the two neighboring values, and then the region is divided into two subdivisions. After n steps, the region has 2^n subdivisions. The value of the newly generated midpoint is,

$$x(t+\delta_{n+1}) = \frac{1}{2}\{x(t) + x(t+\delta_n)\} + \sigma_{\delta n}$$

where $\sigma_{\delta n}$ is a random noise prescribed by the variance of noise after n steps,

$$\sigma_{\delta n}^2 = \sigma_{\delta 0}^2 2^{-2nH}(1 - 2^{2(H-1)})$$

Here, $\sigma_{\delta 0}^2$ is an initial variance. H is called the Hurst index, and has a relation,

$$H = 2 - D_m$$

D_m ($1 < D_m < 2$): fractal dimension of the generalized brownian motion

This method can be extended to producing figures in which dimension is more than 1. For the three dimensional fractal cloud, this cascade process begins with a homogeneous cube, and the cube is to be divided repeatedly into 8 cubes in each step such that 2^{3n} cubes exist after n steps. In the same way as brownian motion, midpoint value is determined with its existing nearest neighbor points either orthogonally or diagonally. In this case, the dimension of the fractal surface is $2 < D_s < 3$.

To apply this procedure to the generation of a three-dimensional cloud, a modification has to be applied. The parameter H in the formulae given above is then set to $H = 3 - D_s$. Axis-parallel and diagonal subdivisions are performed in alternation. For the diagonal subdivision the factor $\sqrt{3}$ is taken into account for the determination of the respective noise variance. Then a cloud with a fractal surface is obtained by setting a certain box-cell threshold. Each box cell is assigned to either empty or cloudy by consulting the threshold according to its value.

The threshold is set so that the volume of the synthesized fractal cloud becomes equal to the cubic clouds to make comparisons. Examples of clouds generated by this way are seen in Fig. 2. Here, clouds with two different fractal scaling factors are shown. In the photon transport simulation, 100 realizations of fractal clouds with H = 0.67 are used.

4. PHOTON TRANSPORT SIMULATION

A radiative transfer model based on the Monte Carlo methpod was applied to both Kosa layer and cloud with fractal scaling nature. In the Monte Carlo method, photons are traced inside the cloud region. Photons are first injected with a given incident angle on the upper plane of the space where clouds are contained. It is assumed that no scatter or absorption takes place while a photon travels in non-cloudy box-cells. Furthermore, reflection and absorption in atmosphere and at the earth's surface are neglected in the process of photon transfer, and a cloud is assumed to be internally homogeneous. Kosa layer is supposed to be horizontally infinite. A photon is only scattered (single scattering albedo equals 1, or no absorption is assumed) in the process of the photon-droplet interaction, and the probability of photon's encounter with a droplet is prescribed by the volume extinction coefficient k. The free path of a photon between one scattering event and the next one is to be described as follows:

$$RN = \exp\left(-\int_0^s k_s \rho ds\right) = \exp\left(-\int_0^s \beta ds\right)$$

,where RN is a random number distributed evenly between 0 and 1 that is created by computer's random generator, ρ is the density of the considering layer, and β is scattering coefficient for a unit volume. Optical depth τ is related to RN as,

$$\tau = \int_0^s \beta ds = -\ln(RN)$$

When a scattering event takes place, the direction of photon progression changes by scattering angle α and azimuthal scattering angle φ. α is determined according to the angular distribution which is controlled by a phase function $p(\alpha)$. The phase function is normalized over solid angle.

The phase function for cumulus cloud is based on Mie scattering calculation with the supposition that the cloud consists of liquid water droplets and the cloud's droplet size distribution is based on Liou's table. The phase function of Kosa is taken from Michenko's ensemble-averaged phase functions for shape distributions of polydisperse, randomly oriented spheroidswith refractive indices and size distributions representative of naturally occurring dust aerosols. φ, the rotation of the axis expressing the direction of propagation before the collision, is given randomly between 0 and 2π.

5. RESULTS

To relate a satellite measurement of reflected radiant intensity, I, to incident solar flux density, F_0, bidirectional reflectance $R(\mu,\phi;\mu_0,\phi_0)$ should be given according to the following formula:

$$R(\mu,\phi;\mu_0,\phi_0) = \frac{\pi I(\mu,\phi)}{\mu_0 F_0(\mu_0,\phi_0)}$$

Provided, the satellite viewing direction makes zenith angle of $\theta = \cos^{-1}\mu$ and azimuthal angle of ϕ . μ_0 and ϕ_0 are for zenith angle and azimuth angle for incident light, respectively.

Fig. 3 exhibits the polar projection of the angular dependence of the bidirectional reflectance function. In these figures, μ=1 is located at the center of each figure, and φ maps to the polar angle, with φ=0 at the top of each figure corresponding back scatter in the solar plane.

As seen in the figures, reflectance becomes higher as zenith angles increases, and the projection of azimuthal reflectance becomes more asymmetric with larger reflectance for φ=0 and φ=180. This effect is mainly due to the fact that side illumination becomes more significant as the solar zenith angle increases. Illumination of the cloud sides allows a fraction of the incident radiation to be backscattered from the sides with angles biased in favor of the normal to the sides. As for Kosa, reflectance is considerablly small but the projection show that back ward scatter is predominant in every solar zenith angle. In case of θ_0 =60, cumulus projection shows the strongest part of reflectance in the angle of 180° As opposed to that, Kosa does not show strong reflectance in the same direction. This is due partly to the fact that volume scattering density of cumulus is about 100 times higher than Kosa, making photon scattering event before it escape from cloud region larger and allowing escaping photons to take various angle other than the angles determined by phase function. On the other hand, Kosa's volume scattering density is quite small, entering photon doesn't have much chance to experience multiple

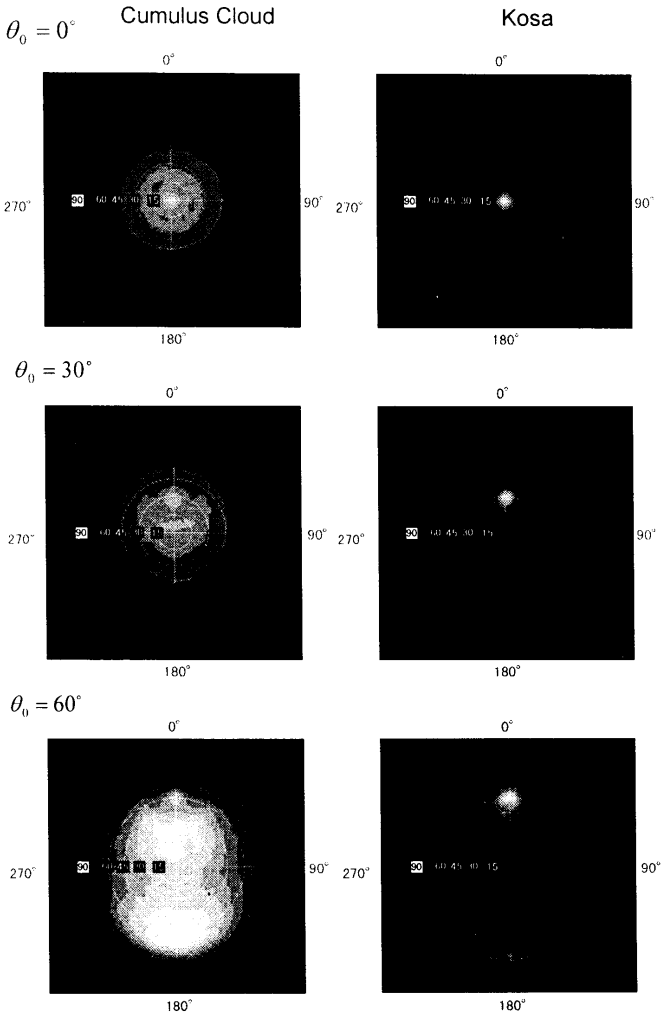

Fig. 3 Bidirectional reflectance function for fractal cloud and Yellow dust

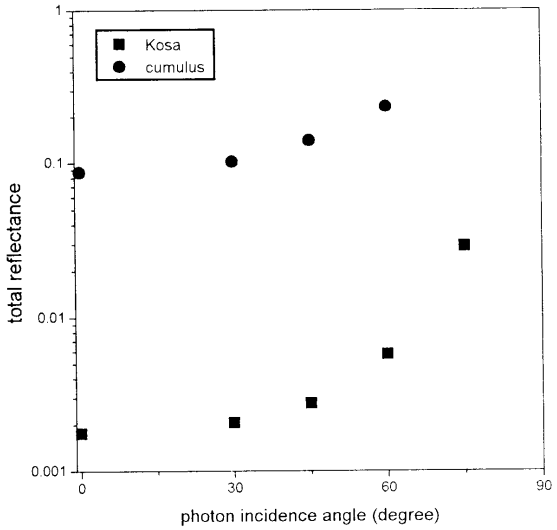

Fig. 4 Total reflectance of cumulus cloud and Kosa as a function of solar zenith angle

scattering, thus the reflectance function become similar to the one determined by phase function, which has higher scattering probability in backward direction.

Fig. 4 shows total reflectance, or total upwelling radiant flux to incident radiant flux, as a function of solar zenith angle. The reflectance increases as zenith angle increases for both cloud and Kosa, which is thought to be for the same aforementioned reason. The degree of increase of total reflectance with zenith angle is higher in Kosa.

References

Aida, M., 1976: Scattering of solar radiation as a function of cloud dimensions and orientation. *J. Quant. Spectrosc. Radiat. Transfer*, **17**. 303-310.

Barker, H. W., 1992: Solar radiative transfer through clouds possessing isotropic variable extinction coefficient. *Q. J. R. Meteorol. Soc.*, **118**, 1145-1162.

Davies, R., 1984: Reflected Solar Radiances from broken cloud scenes and the interpretation of scanner measurements. *J. Geophys. Res.*, **89**, 1259-1266.

Lovejoy, S., 1982: *Area-Perimeter Relation for Rain and Cloud Areas. Science*, **216**, 185-187.

Plank, V. G., 1969: The size distribution of cumulus clouds in representative Florida populations. *J. Appl. Meteor.*, **8**, 46-67.

Liou, K. N., 1992: Radiation and Cloud Processes in the Atmosphere, *Oxford University Press.*.